Biconic Approximation of a Toric Surface

Wei-Jun Chen
R&D Biometry, Ophthalmology, Carl Zeiss Meditec AG, Göschwitzer Straße 51–52, Jena, Germany

Keywords: Biconic Model, Toric Lens, Sphere, Cylinder, Ellipsoid, Elliptic Cylinder, Astigmatism, Approximation.

Abstract: In this work, a toric surface is explicitly approximated by a biconic model by decomposing the toric surface into a biconic–identical component and other elliptical cylinder–related residual components. These residual components determine the zone– and the azimuthal orientation–dependent approximation accuracy. In addition to the analytical underpinning, a direct fit of the biconic model to a data set sampled from a toric surface is performed and consistent results are obtained.

1 INTRODUCTION

In geometrical optics as well as in ophthalmology (cornea), an optical surface with the dominant optical aberration of astigmatism is usually called a toric surface, which has two different refractive powers (refractive curvatures) in two perpendicular meridians, resulting in individual focal lengths.

There are three different but often intermingled descriptions of a toric surface: 1, an optical surface as a "cap" of a torus (Wiki-article, 2023); 2, an optical surface as a composite "spherical + cylindrical" surface (Barcala et al., 1995); 3, an optical surface described by a biconic model with two different radii in two perpendicular axes (e.g., the x– and y–axes).

In general, the first description of the "cap" of a torus is often used to theoretically explain the geometric properties of a toric surface, with the precise mathematical definition being more visually understood (Bartkowska, 1998) (Krasauskas, 2001), while the second description is more of an industry– and market–oriented description that provides an intuitive understanding of the optical behavior of a toric lens. The third description is a more engineering–oriented description that is commonly used for optical design and aberration compensation (Guo and Sun, 2017), lens manufacturing (Chen et al., 2011), clinical trials (Pérez-Escudero et al., 2010) (Janunts et al., 2015) (Moore et al., 2019) (Giraudet et al., 2022) (Langenbucher et al., 2023), scientific research in various fields (Einighammer, 2008) (Gatinel et al., 2011) (Piñero et al., 2012) (Navarro et al., 2019) (Consejo et al., 2021), etc. In addition, optical surfaces with higher complexity, such as aspheres and higher–order freeform surfaces, are often designed based on a toric or biconic model plus additional conical constants and individual Zernike components (Meister, 1998) (Roffman and Menezes, 1998) (Rosales et al., 2009) (Scholz et al., 2009) (Gu et al., 2019) (Brömel, 2018) (Volatier et al., 2020).

Although the three descriptions above differ formally, and have more or less their own flavor, they attempt to provide consistent information about the same optical aberration of astigmatism based on a well–accepted assertion: For a true toric surface, a biconic model with well–determined parameters is a good approximation (Navarro, 2009). Nevertheless, it is not so easy to find in the literature a direct answer to the following question, namely how good such an approximation is, for different specific applications.

An example of this can be found in Fig. 1, where the comparable astigmatism of a toric and a biconic model is illustrated by their refractive power maps in the 12–*mm* zone[1]. However, the toric model also has somewhat "asphericity" inside, while this is not true for the biconic model, although these two models have identical optical and geometric parameters.

With explicitly defined parameters of radius (r_a) and astigmatism (δ) for spherical and cylindrical surfaces, mathematical definitions of the toric surface and the biconic model are rewritten in this paper. Moreover, they are compared and decomposed into their identical part and their distinct components, where these distinct components are analogous to several sums of polynomials of the astigmatism defined elliptic cylinder, which explain well the intrinsic as-

[1]The 12–*mm* and 6–*mm* zones are two typically relevant zones in refractive laser surgery and cataract surgery.

Chen, W.
Biconic Approximation of a Toric Surface.
DOI: 10.5220/0012336800003651

In *Proceedings of the 12th International Conference on Photonics, Optics and Laser Technology (PHOTOPTICS 2024)*, pages 45-50
ISBN: 978-989-758-686-6; ISSN: 2184-4364

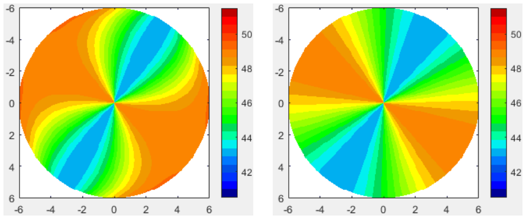

(a) (b)

Figure 1: Refractive power maps of: (a) Toric model; (b) Biconic model. Model parameters: $r_a = 6.88\ mm$, $r_b = 7.85\ mm$, cylinder axis $= 31°$, refractive index $= 1.3375$, map zone $= 12\ mm$, map color unit $= D$ (diopter).

phericity of a standard toric surface, and analytically determine the quality of approximation of a biconic model to a toric surface in a simple way.

The rest of this paper is organized as follows: Sec. 2 rewrites the toric surface and the biconic model with explicit optical parameters; Sec. 3 compares these two models and decomposes them; the quality of approximation of a biconic model to a toric surface is first evaluated analytically in Sec. 4, and then verified in Sec.4.1 by directly fitting a biconic model to a discrete sample set taken from a predefined toric surface; Sec. 5 discusses the evaluation results; finally Sec. 6 concludes this paper with an expectation for future work.

2 TORIC AND BICONIC MODELS

The standard toric surface as "cap" of a torus could be defined by parametric equations[2]

$$\begin{cases} x = (c + a\cos v)\cos u \\ y = (c + a\cos v)\sin u \\ z = a\sin v \end{cases} \tag{1}$$

describing a surface of revolution generated by the rotation of a circle in 3D about the z–axis, where a denotes the radius of the circle, c the decentering of the circle center from the z–axis, v the angular parameter of the points on the circle, and u the angle of rotation.

If we move the coordinate origin to an optical vertex on the surface from $(x,y,z) \to (x, y-(c+a).z)$ and swap the axes y and z as $(x,y,z) \to (x,-z,y)$, we get

$$\begin{cases} x = (c + a\cos v)\cos u \\ z = (c+a) - (c + a\cos v)\sin u \\ y = a\sin v \end{cases} \tag{2}$$

which corresponds to

$$z = (c+a) - \sqrt{\left(c + \sqrt{a^2 - y^2}\right)^2 - x^2} \tag{3}$$

[2]https://mathworld.wolfram.com/Torus.html

and in turn can be rewritten as

$$z = r_a - \sqrt{\left((r_a - r_b) + \sqrt{r_b^2 - y^2}\right)^2 - x^2} \tag{4}$$

where two radii are defined as $r_a = c + a$ and $r_b = a$. Extracting r_a and r_b from two squared root components, we obtain

$$z = r_a\left(1 - \sqrt{1 - \frac{h^2}{r_a^2} + 2\frac{r_b^2}{r_a}\delta\left(1 - \sqrt{1 - \frac{y^2}{r_b^2}}\right)}\right) \tag{5}$$

where $h = \sqrt{x^2 + y^2}$ is the polar radius in the xy plane, and $\delta = \frac{1}{r_a} - \frac{1}{r_b}$ is the astigmatism of the toric surface.

If we continue the *Taylor* expansion for two squared root components in Eq. 5, we obtain:

$$\begin{aligned} z &= \Big(\frac{h^2}{r_a} - \delta y^2 \\ &\quad -2\delta\Big(y^2 \sum_{k=1}^{\infty} p_{k+1}\Big(\frac{y^2}{r_b^2}\Big)^k\Big)\Big) \\ &\quad \times \sum_{m=0}^{\infty} p_{m+1}\Big(\frac{h^2}{r_a^2} + \Delta_r y^2 \\ &\quad + \frac{\delta}{r_b}y^2 - \frac{2\delta}{r_a}\Big(y^2 \sum_{k=1}^{\infty} p_{k+1}\Big(\frac{y^2}{r_b^2}\Big)^k\Big)\Big)^m \end{aligned} \tag{6}$$

where $p_m = \frac{1}{2}, \frac{1}{8}, \frac{1}{16}, \frac{5}{128}, \frac{7}{256}, \ldots$ for $m = 1,2,3,4,5,\ldots$ are polynomial coefficients of $f(x) = 1 - \sqrt{1-x}$, and $\Delta_r = \delta(\delta - \frac{2}{r_a})$ is an astigmatism dependent factor derived from $\frac{1}{r_b^2} = \frac{1}{r_a^2} + \Delta_r$.

On the other hand, the standard biconic model is defined as

$$z = \frac{\frac{x^2}{r_a} + \frac{y^2}{r_b}}{1 + \sqrt{1 - \frac{x^2}{r_a^2}(1+k_a) - \frac{y^2}{r_b^2}(1+k_b)}} \tag{7}$$

where k_a and k_b denote two conic constants and are all zero when only astigmatism is considered. With the above h, δ and Δ_r, Eq. 7 is equivalent to

$$z = \frac{\frac{h^2}{r_a} - \delta y^2}{\frac{h^2}{r_a^2} + \Delta_r y^2}\left(1 - \sqrt{1 - \left(\frac{h^2}{r_a^2} + \Delta_r y^2\right)}\right) \tag{8}$$

which has also its polynomial version:

$$\begin{aligned} z &= \left(\frac{h^2}{r_a} - \delta y^2\right) \\ &\quad \times \sum_{m=0}^{\infty} p_{m+1}\left(\frac{h^2}{r_a^2} + \Delta_r y^2\right)^m . \end{aligned} \tag{9}$$

3 MODEL COMPARISON

Comparing Eq. 6 and Eq. 9, we see that the standard toric surface as a "cap" of a torus contains a biconic part. The Eq. 6 is then rewritten into

$$z = \left(H_\delta - E\right) \times \sum_{m=0}^{\infty} p_{m+1}\left(H_\Delta + \frac{C}{r_b} - \frac{E}{r_a}\right)^m \quad (10)$$

with

$$H_\delta = \frac{h^2}{r_a} - \delta y^2 \quad (11)$$

$$H_\Delta = \frac{h^2}{r_a^2} + \Delta_r y^2 \quad (12)$$

$$C = \delta y^2 \quad (13)$$

$$E = 2C\left(\sum_{k=1}^{\infty} p_{k+1}\left(\frac{y^2}{r_b^2}\right)^k\right) \quad (14)$$

where H_δ and H_Δ contribute to the multiplier and the multiplicand in the biconic model (Eq. 9), and C and E denote a cylinder and an elliptical–cylinder, respectively, inside the toric surface.

4 APPROXIMATION QUALITY

From the above Eqs.10–14, the approximation quality of a biconic model to a toric surface is determined by the cylinder and elliptical–cylinder components inside a toric surface. If we subtract the biconic part from a toric surface, we get the remainder as

$$\begin{aligned} z_{rem} &= z_{toric} - z_{biconic} \\ &= \left(H_\delta - E\right)\left(\sum_{m=1}^{\infty}\sum_{n=1}^{m} p_{m+1} b_{mn} \times \right. \\ &\quad \left. H_\Delta^{m-n}\left(\frac{C}{r_b} - \frac{E}{r_a}\right)^n\right) - \\ &\quad E\left(\sum_{m=0}^{\infty} p_{m+1} H_\Delta^m\right) \end{aligned} \quad (15)$$

where b_{mn} denotes individual binomial coefficients.

The approximation error, i.e., the difference between a biconic model and its approximated toric surface, can be calculated by Eq. 15. To facilitate the analysis of zones and azimuthal orientation, the term y^2 is replaced by $h^2 \sin^2(\rho + \varphi)$ in all equations above, where (h, ρ) denotes the polar coordinates of 2D positions in xy plane and φ the axis orientation of the astigmatism. In the following analysis, the example shown in Fig. 1 is evaluated using Eq. 15, and the approximation error is first illustrated in Fig. 2 for z_{rem} over the whole $12\ mm \times 12\ mm$ region.

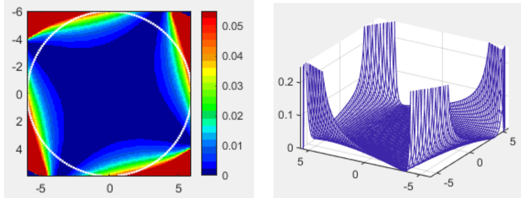

(a) (b)

Figure 2: Approximation error as the difference between a true toric surface and its biconic approximation: (a) Differential map z_{rem}, where the color map illustrates the value range from 0 to $0.05mm$; (b) 3D mesh visualization of the approximation error, where the value range in z axis is from 0 to $0.25mm$.

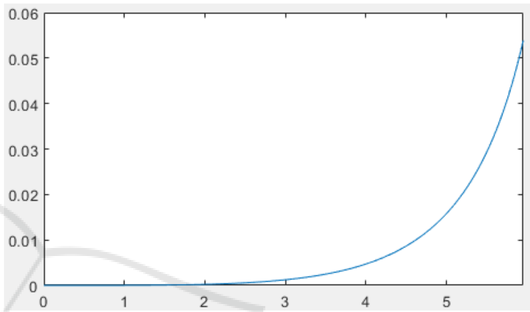

Figure 3: Zone dependence of the approximation error: the curve of $z_{rem}^{max}(h) = \max_\rho\left(z_{rem}(h,\rho)|h \in [0\ 6mm], \rho \in [0^\circ\ 360^\circ]\right)$.

The approximation error of a biconic model to a true toric surface is zone dependent and also depends on the azimuthal orientation. Using the model parameters given in Fig. 1, the zone dependence is illustrated in Fig. 3. From this, it can be seen that the maximum approximation erorr for the example in Fig. 1 is $\approx 0.0012371\ mm$ for a 6–mm zone (i.e., $h \leq 3\ mm$). The dependence on the azimuthal orientation is shown in Fig. 4, where 12 curves of $z_{rem}(h,\rho)$ for individual h values are shown, the horizontal axis being the azimuthal direction from 0° to 360°. It is shown that the approximation error of the evaluated example is lowest along the astigmatism axis φ and its perpendicular axis (i.e., 31° and 121° for the example in Fig. 1), while the maximum error is along the azimuthal orientations of $\varphi \pm 45^\circ$.

The quality of approximation of a biconic model to a true toric surface is also illustrated by the differential refractive power map in Fig. 5, from which we obtain the information that the maximum approximation errors in the 6–mm zone and the 12–mm zone are $\approx 0.36D$ and $\approx 3.22D$, respectively.

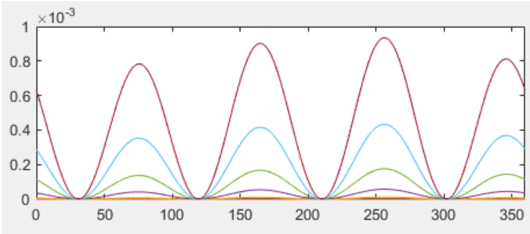

(a)

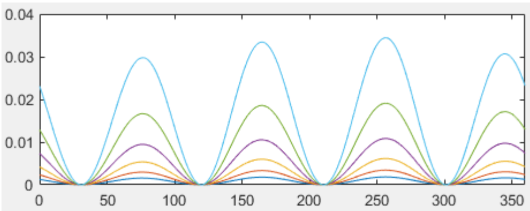

(b)

Figure 4: Azimuthal orientation dependence of the approximation error: the curve of $z_{rem}(h_k, \rho)$ where $h_k = k \times 0.47$ *mm*, and $\rho \in [0° \; 360°)$: (a); 6 curves for $(h_k | k = 0, 1, 2, ...5)$; (b) 6 curves for $(h_k | k = 6, 7, 8...11)$.

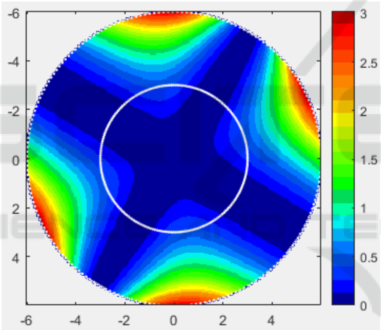

Figure 5: Evaluation of the approximation error by differentiation of two refractive power maps, with two circles drawn in the map to indicate the 6–*mm* zone and the 12–*mm* zone.

4.1 Biconic Model Fitting

In addition to the analytical evaluation of the quality of approximation of a biconical model to a given true toric surface described above, this section describes an experimental evaluation by fitting a biconic model to a discrete sample set, where the sample set $X = (x_i, y_i, z_i | i = 1, 2, ..., N)$ contains a total of 16384 points sampled within an 11–*mm* zone through a regular 128×128 grid with a spatial resolution of 0.09375 *mm* on the *xy* plane, and the *z*–values were calculated using the standard toric model (Eq. 4) with model parameters of the example in Fig. 1. Sampling in the 11–*mm* zone instead of the 12–*mm* zone serves to avoid the surface edge effect.

A non–linear *LeastSquares* fitting was performed based on the standard MATLAB optimization function *lsqcurvefit* and the standard biconic model (Eq. 7). Two model fits were performed, one with the model parameter for (r_a, δ, φ) as a pure astigmatism fit (abbreviation: *A*–fit), and another with all the biconical parameters $(r_a, \delta, \varphi, k_a, k_b)$, namely an astigmatism & conic fit (*AC*–fit).

Table 1: Biconic model fitting results.

Parameters	Truth	*A*–fit	*AC*–fit
r_a (mm)	6.88	6.8660	6.8669
r_b (mm)	7.85	7.8260	7.8755
r_{sph} (mm)	7.365	7.346	7.371
Sph (D)	45.8248	45.9434	45.7875
Cyl (D)	6.0616	6.0298	6.2944
φ $(°)$	31°	31.0001	30.9997
k_a	0	0	-0.0001
k_b	0	0	0.0556
RMS (mm)	0	0.00359	0.00321
Max (mm)	0	0.016	0.015

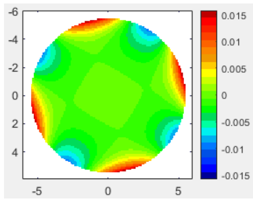

(a)

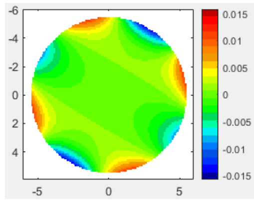

(b)

Figure 6: Fitting error maps: (a) The pure astigmatism fit; (b) The astigmatism & conic fit.

The results of these two model fits are shown in Table 1. From this, we can see that the estimation errors of these two fits for the two perpendicular radii are ≈ -0.014 *mm* for r_a and $\approx \pm 0.025$ *mm* for r_b, while the error for the astigmatism axis is quite small ($\approx 0.0002°$). Moreover, the *AC*–fit is slightly better than the *A*–fit, in terms of the *RMS* criterion, but all *RMS* are > 3 μm for the 11–*mm* zone. Meanwhile, the maximum error in the 11–*mm* zone is about 0.015 *mm*, which is consistent with the analytical evaluation (Fig. 3).

The corresponding 2D error maps for these two fits are shown in Fig. 6. In contrast to the analytical evaluation (Fig. 2), these two model fits produce both positive and negative errors because the *least–squares* optimization is a compromise. For a better understanding of the fitting results, refractive power maps of these two model fits are also shown in Fig. 7. From these two maps, we know that the *A*-fit has the same map structure as the theoretical result (Fig. 5), but with a mean power shift of $\approx +0.12D$, which is consistent with the difference of the equivalence sphere

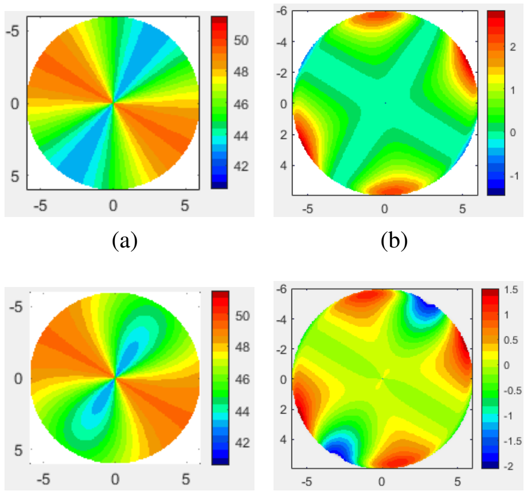

(a) (b) (c) (d)

Figure 7: Model fitting results: (a), The refractive power of the pure astigmatism fit; (b), The differential map as the fitting residual of (a); (c), The refractive power of the astigmatism & conic fit; (d), The differential map as the fitting residual of (c).

(*Sph* in Table 1). On the other hand, the *AC*–fit produces a different power map structure due to the asphericity of two conical constants, which is different from the asphericity resulting from the sums of the polynomials of an elliptical cylinder on the toric surface (Fig. 1(a)).

5 DISCUSSIONS

Based on the above theoretical and experimental underpinning, approximating a biconic model to a toric surface within a bounded zone, such as the 6–*mm* zone for our example surface is good enough. If we go beyond such a bounded zone, the approximation error increases significantly, as shown in Fig. 3 and Fig. 4. On the other hand, the approximation error is theoretically zero along the astigmatism axis and its perpendicular direction, while it periodically increases to a maximum value at $\approx \pm 45°$ from the astigmatism axis. The approximation error is not random noise, but structural deviation; the random noise is generally expected to be suppressed by optimising the model parameters, while the structural deviation is considered to be compensated by model selection and the addition/removal of orthogonal components such as Zernike components.

The interior of a toric surface contains an inherent aspherical component, but it does not seem to be readily described by conical constants in the biconic model, as shown in Fig. 7(c) and Fig. 7(d). Moreover, adjusting the conic constant in the biconic model helps to reduce the RMS very slightly but non–negligibly increases the approximation error of core surface descriptors, such as the spherical radius and the astigmatism, i.e. the *K* (keratometer) and the *Cyl* (cylinder) values in the corneal clinic.

It should be noted that this paper investigates the quality of approximation between two known models with available model parameters, which is only a part of the full solution in many practical applications, e.g., lens quality inspection, refractive modeling of human corneal surfaces, etc. The focus of this work is not to model the measured data by determining optimal parameters for a particular model, but rather to provide a solid basis for the selection of torus or biconical models with similar model parameters for different geometries and refractive requirements.

6 CONCLUSIONS

It turns out that the quality of approximation of the biconical model to a toric surface is good enough within a bounded zone, while outside such a zone the approximation error increases considerably. By representing the standard toric model as a standard biconic model plus remainder components, the approximation error can be calculated analytically using the torus parameters of the base sphere radius, astigmatism, and astigmatism axis. Meanwhile, these remaining components are connected to an elliptical cylinder defined by the toric astigmatism as well as the radius of the base sphere. This creates an intrinsic aspheric structure within the toric surface that does not directly correspond to the ellipsoid–like biconical structure defined by two conical constants.

This work provides a solid foundation for further research on the following three topics: First, from the analysis of the remainder composition (Eq. 15), the approximation acceptable zone should be explicitly determined by the torus parameters of astigmatism and base sphere; second, the choice of the model for given measured data should take into account different geometric structures under the same model parameters, such as different aspherical structures in the toric equation and the biconical equation; third, it has been shown (Eqs. 6 and 9), but not further investigated, that both the toric model and the biconic model are fully compatible with Zernike polynomials. By combining individual Zernike components in different ways, determining model parameters from Zernike coefficients should be suitable for both of the above aspheric structures.

ACKNOWLEDGEMENTS

The author would like to thank his colleagues: Christopher Weth, Tobias Buehen, Ziyao Tang, and Carol Zhang, for their valuable technical discussions.

REFERENCES

Barcala, J., Vazquez, M. C., and Garcia, A. (1995). Optic systems with spherical, cylindrical, and toric surfaces. *Applied Optics*, 34(22):4900–4906.

Bartkowska, J. (1998). Toroidal surfaces in ophthalmic optics. In *Proceedings SPIE: Ophthalmic Measurements and Optometry*, volume 3579, pages 76–93.

Brömel, A. (2018). *Dissertation: Development and evaluation of freeform surface descriptions*. Friedrich–Schiller-Universität Jena, Jena.

Chen, C.-C., Cheng, Y.-C., Hsu, W.-Y., Chou, H.-Y., Wang, P. J., and Tsai, D. P. (2011). Slow tool servo diamond turning of optical freeform surface for astigmatic contact lens. In *Optical Manufacturing and Testing IX*, volume 8126. Proc. of SPIE.

Consejo, A., Fathy, A., Lopes, B. T., Renato Ambrósio, J., and Abass, A. (2021). Effect of corneal tilt on the determination of asphericity. *Sensors*, 21(22):1–15.

Einighammer, J. (2008). *Dissertation: The Individual Eye*. Eberhard-Karls-Universität Tübingen, Tübingen.

Gatinel, D., Malet, J., Hoang-Xuan, T., and Azar, D. T. (2011). Corneal elevation topography: Best fit sphere, elevation distance, asphericity, toricity and clinical implications. *Cornea*, 30(5):508–515.

Giraudet, C., Diaz, J., Tallec1, P. L., and Allain1, J.-M. (2022). Multiscale mechanical model based on patient-specific geometry: application to early keratoconus development. *Journal of the Mechanical Behavior of Biomedical Materials*, 129:1–13.

Gu, Y., McKenney, C. D., and Niculas, C. D. (2019). Method for manufacturing toric contact lenese. *US Patent Application: US 2019/0193350 A1*.

Guo, Y. and Sun, L. (2017). Biconic white multipass cell design based on a skew ray–tracing model. *Applied Optics*, 56(27):7586–7595.

Janunts, E., Kannengießer, M., and Langenbucher, A. (2015). Parametric fitting of corneal height data to a biconic surface. *Zeitschrift für Medizinische Physik*, 25(1):25–35.

Krasauskas, R. (2001). Shape of toric surfaces. In *Proceedings Spring Conference on Computer Graphics*, pages 55–62.

Langenbucher, A., Szentmáry, N., Cayless, A., Muenninghoff, L., Wylegala, A., Wendelstein, J., and Hoffmann, P. (2023). Bootstrapping of corneal optical coherence tomography data to investigate conic fit robustness. *Journal of Clinical Medicine*, 12:1–16.

Meister, D. (1998). Principles of atoric lens design. *Lens Talk*, 27(03):1–4.

Moore, J., Shu, X., Lopes, B. T., Wu, R., and Abass, A. (2019). Limbus misrepresentation in parametric eye models. *PLoS ONE*, 15(9):1–22.

Navarro, R. (2009). The optical design of the human eye: a critical review. *Journal of Optometry*, 2(1):3–18.

Navarro, R., Rozema, J., Emamian, M. H., Hashemi, H., and Fotouhi, A. (2019). Average biometry of the cornea in a large population of iranian school children. *Journal of the Optical Society of America A: Optics, Image Science, and Vision*, 36(4):B85–B92.

Pérez-Escudero, A., Dorronsoro, C., and Marcos, S. (2010). Correlation between radius and asphericity in surfaces fitted by conics. *Journal of the Optical Society of America A*, 27(7):1541–1548.

Piñero, D. P., Nieto, J. C., and Lopez-Miguel, A. (2012). Characterization of corneal structure in keratoconus. *Journal of Cataract & Refractive Surgery*, 38:2167–2183.

Roffman, J. H. and Menezes, E. V. (1998). Aspheric toric lens designs. *US Patent: US 5796462*.

Rosales, M. A., Juárez-Aubry, M., López-Olazagasti, E., Ibarra, J., and Tepichín, E. (2009). Anterior corneal profile with variable asphericity. *Applied Optics*, 48(35):6594–6599.

Scholz, K., Messner, A., Eppig, T., Bruenner, H., and Langenbucher, A. (2009). Topography-based assessment of anterior corneal curvature and asphericity as a function of age, sex, and refractive status. *Journal of Cataract & Refractive Surgery*, 35:1046–1054.

Volatier, J.-B., Duveau, L., and Druart, G. (2020). An exploration of the freeform two–mirror off–axis solution space. *Journal of Physics: Photonics*, 2:1–9.

Wiki-article (2023). Toric lens. *https://en.wikipedia.org/wiki/Toric_lens*.